

ADAPTIVE CONTROL FOR THE CONVENTIONAL MODE OF OPERATION OF MEMS GYROSCOPES

Sungsu Park and Roberto Horowitz

* *PATH, University of California, Berkeley, CA 94720*

** *Dept. of Mechanical Engineering, University of
California, Berkeley, CA 94720*

Abstract: This paper presents adaptive add-on control algorithms for the conventional mode of operation of MEMS z-axis gyroscopes. This scheme is realized by adding an outer loop to a conventional force-balancing scheme that includes a parameter estimation algorithm. The parameter adaptation algorithm estimates the angular rate, identifies and compensates the quadrature error, and may permit on-line automatic mode tuning with no measurement of input/output phase difference. The convergence and resolution analysis show that the proposed adaptive add-on control scheme prevents the angular rate estimate from being contaminated by the quadrature error, while keeping ideal resolution performance of a conventional force-balancing scheme.

Keywords: MEMS, gyroscope, adaptive control, force-balancing control, averaging analysis

1. INTRODUCTION

Most MEMS gyroscopes are vibratory rate gyroscopes that have structures fabricated on polysilicon or crystal silicon, and mechanical main component is a two degree-of-freedom vibrating structure, which is capable of oscillating on two directions in a plane. Their operating physics is based on the Coriolis effect. When the gyroscope is subjected to an angular velocity, the Coriolis effect transfers energy from one vibrating mode to another. The response of the second vibrating mode provides information about the applied angular velocity. Ideally in the conventional mode of operation, the vibrating modes of a MEMS gyroscope are supposed to remain mechanically uncoupled, their natural frequencies should be matched, and the gyroscope's output should only be sensitive to angular velocity [1]. In practice however, fabrication imperfections and environment variations are always present, resulting in a frequency of oscilla-

tion mismatch between the two vibrating modes and a coupling between the two mechanical vibration modes through off-diagonal terms in the stiffness and damping matrices. These imperfections degrade the gyroscope's performance and cause a false output [2]. As a consequence, some kind of control is essential for improving the performance and stability of MEMS gyroscopes, by effectively cancelling "parasitic" effects. For a closed-loop mode of operation, two feedback control methods have been presented in the literature that compensate fabrication imperfections and measure angular velocity. One is a Kalman filter based preview control [3] and the others are force-balancing feedback control schemes [4]. Although these feedback control techniques increase the bandwidth and dynamic range of the gyroscope beyond the open-loop mode of operation, they still are sensitive to parameter variations, and angular rate estimate may be contaminated by the quadrature error. In

this paper, we develop an adaptive add-on control scheme for operating a MEMS z-axis gyroscope in conventional force-balancing mode. This adaptive algorithm estimates the angular rate and, at the same time, identifies and compensates quadrature error, and may permit on-line automatic mode tuning. In the next sections, the dynamics of MEMS gyroscopes is developed by accounting for the effect of fabrication imperfections. The force-balancing control scheme is reviewed in section 3. In section 4, an adaptive add-on control approach is developed as an extension of conventional force-balancing control scheme, and the convergence and resolution analysis of the proposed adaptive add-on controlled gyroscope is presented. Finally, computer simulations are performed in section 5.

2. DYNAMICS OF MEMS GYROSCOPES

Common MEMS vibratory gyroscope configurations include a proof mass suspended by spring suspensions, and electrostatic actuations and sensing mechanisms for forcing an oscillatory motion and sensing the position and velocity of the proof mass. These mechanical components can be modelled as a mass, spring and damper system. Figure 1 shows a simplified model of a MEMS gyroscope having two degrees of freedom in the associated Cartesian reference frames.

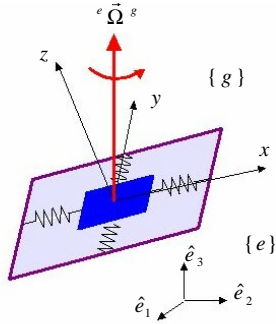


Fig. 1. A model of a MEMS z-axis gyroscope

Assuming that the motion of the proof mass is constrained to be only along the x - y plane by making the spring stiffness in the z direction much larger than in the x and y directions, the measured angular rate is almost constant over a long enough time interval, and linear accelerations are cancelled out, either as an offset from the output response or by applying counter-control forces, then the equation of motion of a gyroscope is given as follows with taking into account fabrication imperfections which always occur in practice.

$$\begin{aligned} m\ddot{x} + d_{xx}\dot{x} + d_{xy}\dot{y} + k_{xx}x + k_{xy}y &= \tau_x + 2m\Omega_z\dot{y} \\ m\ddot{y} + d_{xy}\dot{x} + d_{yy}\dot{y} + k_{xy}x + k_{yy}y &= \tau_y - 2m\Omega_z\dot{x} \end{aligned} \quad (1)$$

where x and y are the coordinates of the proof mass relative to the gyro frame, $d_{xx,yy}$ and $k_{xx,yy}$ are damping and spring coefficients, Ω_z are the angular velocity components along z -axis of the gyro frame and $\tau_{x,y}$ are control forces. The two last terms in equation (1), $2m\Omega_z\dot{y}$ and $2m\Omega_z\dot{x}$ are due to the Coriolis forces. Fabrication imperfections contribute mainly to the asymmetric spring and damping terms, k_{xy} and d_{xy} . Therefore these terms are unknown, but can be assumed to be small. The x and y axes spring and damping terms are mostly known, but have small unknown variations from their nominal values. The proof mass can be determined very accurately. The components of angular rate along x and y axes are absorbed as part of the spring terms as unknown variations. Note that the spring coefficients k_{xx} and k_{yy} also include the electrostatic spring softness.

3. CLOSED-LOOP MODE OF OPERATION

Conventional mode of operation is classified by an open-loop mode and a closed-loop mode. The major difference between the closed-loop and open-loop mode of operation lies in that in the former the displacement of the sense axis is controlled to zero, while in the latter it is measured. The process of conventional mode of operation is based on the following equation:

$$\begin{aligned} x &= X_0 \sin(\omega_x t) \\ \ddot{y} + \frac{\omega_y}{Q_y}\dot{y} + \omega_y^2 y &= \tau_y - \omega_{xy}x - (d_{xy} + 2\Omega_z)\dot{x} \end{aligned} \quad (2)$$

where $\omega_x = \sqrt{\frac{k_{xx}}{m}}$, $\omega_y = \sqrt{\frac{k_{yy}}{m}}$, $\omega_{xy} = \frac{k_{xy}}{m}$, $d_{xy} \leftarrow \frac{d_{xy}}{m}$, Q_y is the y -axis quality factor, and X_0 is the amplitude of x -axis oscillation.

The force-balancing control strategy was originally developed for MEMS accelerometer control [5], where it has been successfully applied, and it has been extended to MEMS gyroscopes [4]. The basic idea behind the force-balancing control strategy is that, if the sense mode amplitude is regulated to zero by feedback control action, then, since $\ddot{y} \approx \dot{y} \approx y \approx 0$, equation (2) yields in steady-state response,

$$\tau_y = \omega_{xy}x + (d_{xy} + 2\Omega_z)\dot{x} \quad (3)$$

This implies that applied angular rate Ω_z can in principle be inferred from the sense axis control output τ_y , under the assumption that $d_{xy} = 0$. The force-balancing control strategy requires that the sense axis closed loop system be robust to parameter uncertainties and variations, and have minimal phase shift so that the response of the system to the Coriolis acceleration and quadrature error can be distinguishable.

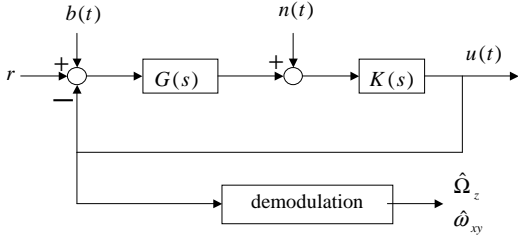


Fig. 2. Block diagram of the force-balancing control

A block diagram of a sense axis force-balancing control is shown in Figure 2. $G(s)$ is the sense axis gyroscope dynamics, $K(s)$ is the compensator which will be subsequently designed, $r = -2\Omega_z\omega_x X_0 \cos(\omega_x t) - \omega_{xy} X_0 \sin(\omega_x t)$ is the modulated input signal resulting from the Coriolis acceleration and quadrature error, $u = \tau_y$ is the control output, n is the measurement noise, and b is the Brownian input noise. Figure 2 also includes a demodulation block. The closed loop sensitivity transfer functions for u and y are given by

$$\begin{aligned} u(s) &= T(s)(r + b) + S(s)n \\ y(s) &= V(s)(r + b) - T(s)n \end{aligned} \quad (4)$$

where

$$\begin{aligned} T(s) &= \frac{K(s)G(s)}{1 + K(s)G(s)}, \quad S(s) = \frac{K(s)}{1 + K(s)G(s)} \\ V(s) &= \frac{G(s)}{1 + K(s)G(s)} \end{aligned}$$

The control design goal is to flatten the gain of the complementary sensitivity function $T(s)$ for u around the drive axis frequency ω_x , i.e.

$$|T(j\omega)| \approx \text{const}, \quad \text{for } \omega \in [\omega_x - \Delta\omega, \omega_x + \Delta\omega]$$

The compensator $K(s)$ may be designed by various methods such as μ -synthesis and H^∞ for stability robustness, or using classical control synthesis techniques. If the magnitude of the closed-loop complementary transfer function $T(s)$ from the angular rate to the control output is flat around the drive axis frequency, the gyroscope's scale factor will remain constant in the presence of drive or sense axis frequency variations. Moreover, the gyroscope's bandwidth can be increased up to the drive axis frequency. The dynamic range and linearity are also improved to the extent of the control authority, since the magnitude of the sensitivity transfer function $V(s)$ from the angular rate to the sense axis displacement is almost zero. Since, by equation (4), the steady-state control signal u contains both the Coriolis and quadrature error signals, a demodulation is needed for extracting angular velocity information from the control signal. Eventually, the overall gyroscope performance will depend on the demodulation method used. Suppose that the phase delay is small around the anticipated drive frequency region, then the angular rate and quadrature er-

ror may be demodulated from the control output by multiplying this signal by $\cos \omega_x t$ and $\sin \omega_x t$, and filtering the resulting signals with a low-pass filter. However, unless the ϕ_{quad} is exactly zero, the estimation of angular rate is contaminated by the unknown quadrature error coupling term ω_{xy} . Unfortunately, usually the quadrature error is 3 or 4 orders of magnitude larger than the angular rate. Although the quadrature error term can potentially be cancelled out by initial calibration, it may vary during the operation of the gyroscope.

4. ADAPTIVE ADD-ON CONTROL

We investigate the use of an adaptive algorithm for estimating angular rate and at the same time, identifying and compensating quadrature error, and possibly attaining mode match in an on-line fashion. Note that the effect of variations in drive or sense axis frequencies is not observed explicitly in the control output of a conventional force-balancing system. The idea behind the use of adaptive add-on control is to make the nominal control output of the conventional force-balancing system equal to zero by adding an additional outer loop. The add-on control outer loop is composed of a band-pass filter, a parameter adaptation law and a modulation part. Figure 3 shows a block diagram of force-balancing system with the adaptive add-on control.

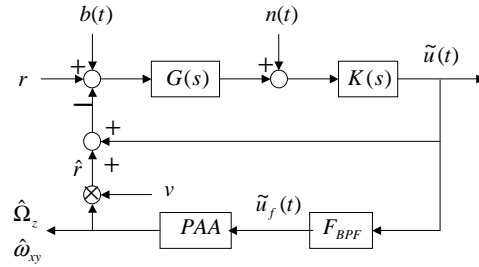


Fig. 3. Block diagram of the adaptive add-on control

The modulated input signal r in the equation (4) is re-written in regressor form as

$$r = -2\Omega_z \dot{x} - \omega_{xy} x = -\theta^T v \quad (5)$$

where $\theta = [2\Omega_z \ \omega_{xy}]^T$ is assumed to be an unknown parameter and $v = [\dot{x} \ x]^T$ is the measurable regressor. Suppose that the input signal r is estimated by a parameter adaptation algorithm, then its estimate signal and errors are

$$\begin{aligned} \hat{r} &= -2\hat{\Omega}_z(t)\dot{x} - \hat{\omega}_{xy}(t)x = -\hat{\theta}^T v \\ \tilde{r} &= r - \hat{r} = 2\tilde{\Omega}_z(t)\dot{x} + \tilde{\omega}_{xy}x = \tilde{\theta}^T v \end{aligned} \quad (6)$$

where the parameter estimate errors are $\tilde{\Omega}_z = \hat{\Omega}_z - \Omega_z$, $\tilde{\omega}_{xy} = \hat{\omega}_{xy} - \omega_{xy}$ and $\tilde{\theta} = \hat{\theta} - \theta$. The control error dynamics \tilde{u} is

$$\begin{aligned}\tilde{u} &= T(r + b - \hat{r}) + S(n) \\ &= T(\tilde{\theta}^T v) + T(b) + S(n)\end{aligned}\quad (7)$$

If the error signal \tilde{u} passes through a band-pass filter $F_{BPF}(s)$, then

$$\begin{aligned}\tilde{u}_f &= F_{BPF}(\tilde{u}) \\ &= T_{BPF}(\tilde{\theta}^T v) + T_{BPF}(b) + S_{BPF}(n)\end{aligned}\quad (8)$$

where $T_{BPF}(s) = F_{BPF}(s)T(s)$ and $S_{BPF}(s) = F_{BPF}(s)S(s)$. The following theorem holds.

Theorem: Assume that Ω_z and ω_{xy} are constant. Suppose that a conventional force-balancing closed loop system is stable with a controller $K(s)$. If a band-pass filter is designed such that the phase delay from the modulated input signal r to the output of a band-pass filter is less than 90° for a drive axis frequency ω_x , and the parameter estimates $\hat{\Omega}_z$ and $\hat{\omega}_{xy}$ are updated by the following adaptation laws:

$$\begin{aligned}\dot{\hat{\Omega}}_z &= -\gamma_\Omega \tilde{u}_f \dot{x} \\ \dot{\hat{\omega}}_{xy} &= -\gamma_\omega \tilde{u}_f x\end{aligned}\quad (9)$$

then the angular rate Ω_z and quadrature error ω_{xy} can be estimated correctly, i.e. $\tilde{\Omega}_z \rightarrow 0$, $\tilde{\omega}_{xy} \rightarrow 0$, where γ_Ω and γ_ω are positive adaptation gains.

Proof: Since the propagation equation of the stochastic expectation has the same form as the deterministic counterpart, we can consider the deterministic case, i.e. $b = 0$ and $n = 0$. Usually, $T(s)$ and $T_{BPF}(s)$ are not SPR (strictly positive real), so it is difficult to prove the stability of the closed-loop system with an adaptation loop. Here, we make use of the fact that the driving signal is a single frequency sinusoid, and take an averaging approach [6]. Assuming that the applied angular rate and quadrature error are constant, then equation (9) is equal to

$$\dot{\tilde{\theta}} = - \begin{bmatrix} 2\gamma_\Omega & 0 \\ 0 & \gamma_\omega \end{bmatrix} \begin{bmatrix} X_0 \omega_x \cos(\omega_x t) \\ X_0 \sin(\omega_x t) \end{bmatrix} \tilde{u}_f \quad (10)$$

Assuming that estimate error dynamics $\tilde{\theta}$ is slow, from equation (8), the steady state dynamics of \tilde{u}_f is approximately given by

$$\begin{aligned}\tilde{u}_f &\approx T_{BPF}(v^T) \tilde{\theta} = |T_{BPF}(\omega_x)| \\ &\cdot [X_0 \omega_x \cos(\omega_x t + \phi) \quad X_0 \sin(\omega_x t + \phi)] \tilde{\theta}\end{aligned}\quad (11)$$

where ϕ is a phase delay from the modulated input signal r to the output of the band-pass filter. Substituting (11) into (10) and taking averages result in

$$\begin{bmatrix} \dot{\tilde{\Omega}}_z \\ \dot{\tilde{\omega}}_{xy} \end{bmatrix}_{AVG} = - |T_{BPF}(\omega_x)| X_0^2 R_{\Omega\omega} \begin{bmatrix} \tilde{\Omega}_z \\ \tilde{\omega}_{xy} \end{bmatrix}_{AVG}\quad (12)$$

where

$$R_{\Omega\omega} = \begin{bmatrix} \gamma_\Omega \omega_x^2 \cos \phi & -\gamma_\Omega \omega_x \sin \phi \\ 1 & \frac{1}{2} \\ \frac{1}{2} \gamma_\omega \omega_x \sin \phi & \frac{1}{2} \gamma_\omega \cos \phi \end{bmatrix}$$

We have used the fact that the products of sinusoids at different frequencies have zero average. A sufficient condition for the system in the equation (12) to be asymptotically stable is that the cross-correlation matrix $R_{\Omega\omega}$ be positive-definite. This is achieved if $\cos \phi > 0$. Therefore, if $-90^\circ < \phi < 90^\circ$, the convergence of parameter errors to zero is guaranteed, and the stability of the system is proven.

If we carefully design a compensator $K(s)$ and a band-pass filter $F_{BPF}(s)$ so that phase delay is as small as possible, the angular rate estimate dynamics will be almost decoupled from that of the quadrature error estimate. In this case, the quadrature error estimation transient response will not significantly affect the transient response of the angular rate estimate and vice versa. Although the quadrature error estimate dynamics affects that of the angular rate estimate, this only happens during the transient period. This is the main advantage of this scheme over the conventional force-balancing control, where the angular rate estimate is contaminated by the quadrature error term, unless it is perfectly compensated. This control provides the quadrature compensation and closed-loop identification of the angular rate with no measurement of input/output phase difference.

4.1 Performance Expectation

The bandwidth of a conventional force-balancing controlled gyroscope is defined by the cut-off frequency of the low-pass filter used in the demodulation process. On the other hand, the bandwidth of the proposed force-balancing controlled gyroscope with adaptive add-on control is defined by the adaptation gain γ_Ω . From equation (12), assuming that $\phi \approx 0$, its bandwidth can be estimated by

$$BW \approx \gamma_\Omega |T_{BPF}(\omega_x)| X_0^2 \omega_x^2 \quad (13)$$

Of course, the actual maximum bandwidth is also limited by the band-pass filter. Therefore, the adaptation gain γ_Ω should be selected so that the bandwidth estimate given by equation (13) is lower than half of the frequency pass-band of the band-pass filter.

In the case of the adaptive add-on control, resolution is a function of the adaptation gain γ_Ω and the pass-band of the band-pass filter $F_{BPF}(s)$. In order to accurately estimate resolution of nominal system, consider the following state-space realization of $T_{BPF}(s)$ and $S_{BPF}(s)$:

$$\begin{aligned}T_{BPF}(s) &: (A_T, B_T, C_T) \\ S_{BPF}(s) &: (A_S, B_S, C_S)\end{aligned}$$

Then, the equations (11) and (12) are realized the following state-space form.

$$\begin{bmatrix} \dot{x}_e \\ \dot{\theta} \end{bmatrix} = \begin{bmatrix} A_{11} & A_{12} \\ A_{21} & 0 \end{bmatrix} \begin{bmatrix} x_e \\ \theta \end{bmatrix} + \begin{bmatrix} B_1 \\ 0 \end{bmatrix} \begin{bmatrix} b \\ n \end{bmatrix} \quad (14)$$

where

$$A_{11} = \text{diag}\{A_T, A_T, A_S\}, \quad A_{21} = -\gamma v [C_T \ C_T \ C_S]$$

$$A_{12} = \begin{bmatrix} B_T v^T \\ 0 \end{bmatrix}, \quad B_1 = \begin{bmatrix} 0 & 0 \\ B_T & 0 \\ 0 & B_S \end{bmatrix}$$

$$\gamma = \text{diag}\{2\gamma_\Omega, \gamma\omega\}, \quad v = [\dot{x} \ x]^T$$

The covariance of $[x_e^T \ \tilde{\theta}^T]^T$ can be computed by solving the following covariance propagation equation.

$$\dot{P} = PA^T + AP + BSB^T \quad (15)$$

where $S = \text{diag}\{S_b, S_p\}$. The standard deviation of the angular rate estimate error, or resolution σ_Ω , is obtained from the covariance matrix P , and is computed by

$$\sigma_\Omega = \sqrt{CPC^T} \quad (16)$$

where $C = [0_{1 \times m} \ 1]$, and m is a dimension of P .

Now, we investigate a relationship of resolution performance between conventional force-balancing and adaptive add-on force-balancing schemes. If we substitute equation (8) to (10), then

$$\dot{\tilde{\theta}} = -\gamma v T_{BPF}(v^T \tilde{\theta}) - \gamma v T_{BPF}(b) - \gamma v S_{BPF}(n) \quad (17)$$

The stochastic expectation equation of (17) is given by $E[\dot{\tilde{\theta}}] = -\gamma v T_{BPF}(v^T E[\tilde{\theta}])$, where $E[\cdot]$ denotes stochastic expectation. Define the expectation error as $\check{\theta} = \tilde{\theta} - E[\tilde{\theta}]$, then

$$\begin{aligned} \dot{\check{\theta}} &= -\gamma v T_{BPF}(v^T \check{\theta}) - \gamma v T_{BPF}(b) - \gamma v S_{BPF}(n) \\ &\approx -\gamma v T_{BPF}(v^T) \check{\theta} - \gamma v T_{BPF}(b) - \gamma v S_{BPF}(n) \end{aligned} \quad (18)$$

where we have utilized the assumption that the dynamics of $\check{\theta}$ is slow. Thus, the transfer function from noises to $\check{\theta}$ is given by

$$\begin{aligned} \check{\theta}(s) &= -(sI + \gamma v T_{BPF}(v^T))^{-1} \gamma v T_{BPF}(b) \\ &\quad - (sI + \gamma v T_{BPF}(v^T))^{-1} \gamma v S_{BPF}(n) \end{aligned} \quad (19)$$

If we assume phase delay $\phi \approx 0$ and consider only the angular rate part, then equation (19) is simplified as

$$\begin{aligned} \check{\Omega}_z(s) &\approx -\frac{1}{X_0 \omega_x |T_{BPF}(\omega_x)|} \frac{BW}{s + BW} \\ &\quad \cdot \cos(\omega_x t) (T_{BPF}(b) + S_{BPF}(n)) \end{aligned} \quad (20)$$

Equation (20) can be interpreted as follows: The noise that contaminates the angular rate estimate is a low-pass filtered signal of the demodulated noise signals, passed through shaping filters $T_{BPF}(s)$ and $S_{BPF}(s)$. These are the same

noise properties observed in a conventional force-balancing control using a demodulation process.

Because the shape of the frequency response of $S(s)$ is the inverse of that of $G(s)$, the power of the noise in band-pass filtered control output signal \tilde{u}_f is minimal when $\omega_x = \omega_y$. Thus, the mode tuning problem may be formulated as follows:

$$\omega_y^* = \arg_{\omega_y} \min E[\tilde{u}_f^2] \quad (21)$$

where $E[\cdot]$ stands for the stochastic expectation. Note that the noise properties of the angular rate estimate such as standard deviation can easily be calculated by measuring control output signal \tilde{u}_f .

5. SIMULATIONS

A simulation study using the preliminary design data of the MIT-SOI MEMS gyroscope was conducted, to test the analytical results and verify the predicted performance of the adaptive add-on controlled gyroscope presented in this paper. We assumed that the drive and sense axis resonant frequencies are matched and the magnitude of quadrature error is 0.1% of nominal resonant frequency. The data of some of the gyroscope parameters in the model is summarized in Table 1. Notice that the simulation results are shown in non-dimensional units, which are non-dimensionalized based on the proof-mass, length of one micron and the x -axis nominal natural frequency.

The estimate of the angular rate response to the step input angular rate is shown in Figure 4. In this figure, the upper and lower bounds of the analytically estimated standard deviation are also plotted. The estimated standard deviation with equation (16) is 0.56 *deg/sec* at 50 *Hz* of bandwidth. Figure 5 shows the estimate of angular rate response to the sinusoidal input angular rate, and Figure 6 shows the time response of the quadrature error estimate. These simulation results well match the theoretical results obtained in this paper.

Table 1. Key parameters of the gyroscope

parameter	value
mass	$5.095 \times 10^{-7} \text{ kg}$
x -axis frequency	4.17 <i>KHz</i>
Quality factor	40
Brownian noise PSD	$5.53 \times 10^{-24} \text{ N}^2 \text{ sec}$
Position noise PSD	$1.49 \times 10^{-27} \text{ m}^2 \text{ sec}$

6. CONCLUSIONS

For a closed-loop mode of operation, an adaptive add-on control scheme was proposed. The idea behind this add-on control is to achieve a zero

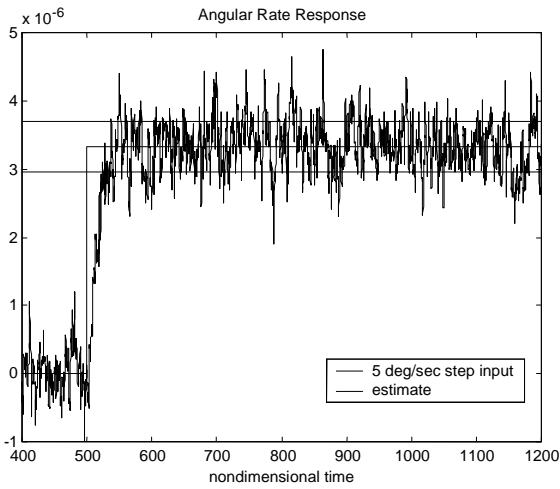


Fig. 4. Time response of angular rate estimate to the 5 deg/sec step input

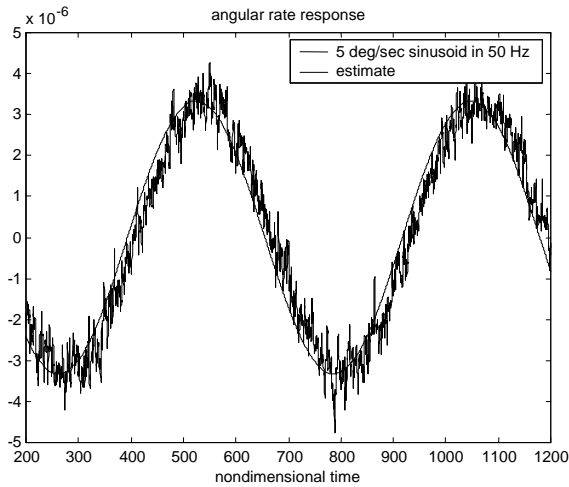


Fig. 5. Time response of angular rate estimate to the 5 deg/sec sinusoid input at 50 Hz

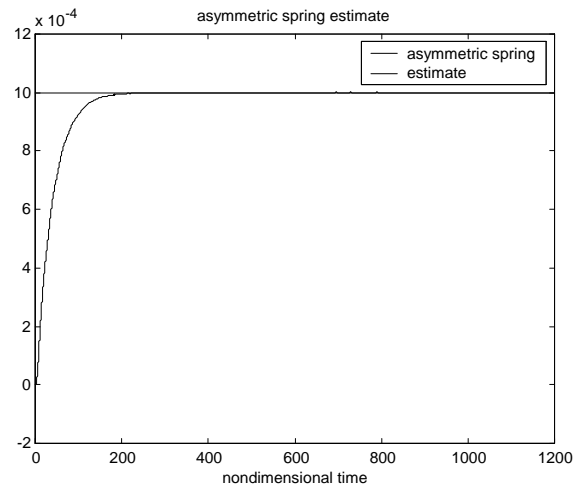


Fig. 6. Time response of quadrature error estimate

nominal control output in a conventional force-balancing system by adding an additional outer loop. The proposed outer loop is composed of a band-pass filter, a parameter adaptation algorithm, and an algorithm that generates estimates of the gyroscopic inputs and other perturbation

inputs due to fabrication defects. This parameter adaptation algorithm estimates the angular rate and, at the same time, identifies and compensates quadrature error, and may permit on-line automatic mode tuning with no measurement of input/output phase difference.

The convergence and resolution analysis of the adaptive add-on controlled gyroscope was presented. This analysis shows that the proposed adaptive add-on control scheme prevents the angular rate estimate from being contaminated by the quadrature error, while keeping ideal resolution performance of a conventional force-balancing scheme. Simulation results were presented which corroborate the analytically derived performance. However, both the open-loop and closed-loop modes are inherently sensitive to some types of fabrication imperfections which can be modelled as cross-damping terms, which produce zero-rate output.

ACKNOWLEDGEMENTS

This research was supported by DARPA under Contract N66001-97-C-8643.

REFERENCES

- [1] N. Yazdi, F. Ayazi and K. Najafi, "Micromachined Inertial Sensors", *Proceedings of IEEE*, Vol.86, No.8, pp.1640-1659, August 1998.
- [2] A. Shkel, R.T. Howe and R. Horowitz, "Modeling and simulation of micromachined gyroscopes in the presence of imperfection", *Int. Conf. On Modelling and Simulation of Microsystems*, Puerto Rico, pp. 605-608, 1999.
- [3] P.B. Ljung, *Micromachined Gyroscope with Integrated Electronics*, Doctoral Thesis, U.C. Berkeley, 1997.
- [4] X. Jiang, J. Seeger, M. Kraft and B.E. Boser, "A monolithic surface micromachined Z-axis gyroscope with digital output", *IEEE 2000 Symposium on VLSI Circuits*, Honolulu, HI, pp.16-19, June 2000.
- [5] C. Lu, M. Lamkin and B.E. Boser, "A Monolithic Surface Micromachined Accelerometer with Digital Output", *IEEE Journal of Solid-State Circuits*, Vol.30, No.12, pp.1367-1373, Dec. 1995.
- [6] S.S. Sastry, *Adaptive Control: Stability, Convergence and Robustness*, Prentice Hall, 1989.
- [7] S. Park, *Adaptive Control Strategies for MEMS Gyroscopes*, Doctoral Thesis, U.C. Berkeley, 2000.
- [8] W.A. Clark, *Micromachined Vibratory Rate Gyroscopes*, Doctoral Thesis, U.C. Berkeley, 1997.